Camila R. de Lacerda[1,2,*]
Peter Bächler[2]
Almuth D. Schwarz[2]
Rafael Sartim[3,4]
Mônica L. Aguiar[1]
Achim Dittler[2]

Impact of Seams on the Operating Behavior of Surface Filters Regarding Particle Emissions

Surface filters are widely used in industrial gas cleaning, e.g., as filter bags, to meet particle emission standards. The seam created by manufacturing the filter element is a potential leakage point for dust. A systematic investigation on the impact of the needle diameter of the seam on filter operation in two different filter test rigs is presented, regarding differential pressure and particle emissions. Four membrane samples, one without seam and three sewn with different needle diameters, were used to evaluate the fractional separation efficiency and the dust emissions. While the sample without seam showed near-perfect particle separation, a larger needle diameter led to an increase in dust emissions. The impact of needle diameter on the differential pressure was negligible.

Keywords: Baghouse filter, Filter seams, Needle diameter, Particle emissions, Surface filter

Received: March 11, 2022; *revised:* May 05, 2022; *accepted:* May 17, 2022

DOI: 10.1002/ceat.202200132

Supporting Information available online

1 Introduction

Particulate emission control is a matter of great concern worldwide, as inhalation of fine particles due to air pollution has been linked to respiratory and heart disease, neurodegenerative disorders, stroke, and cancer [1–3]. Regarding particle emission limits, the environmental legislation is becoming stricter by the day. As an example, Germany has an air pollution control regulation referred to as "technische Anleitung (TA) Luft" which sets limits for dust emissions to the maximum concentration of 20 mg m^{-3} [4]. In Brazil, the air quality standards are established by the Conselho Nacional de Meio Ambiente (CONAMA), Resolution no. 491/2018 [5]. The first phase of the plan recommends that all states should achieve annual air pollution limits of 40 µg m^{-3} for PM10 and 20 µg m^{-3} for PM2.5. The final phase of this plan will require states to limit their annual emissions to meet the ambient particle concentration limits recommended by the World Health Organization in 2005 [6], 20 µg m^{-3} for PM10 and 10 µg m^{-3} for PM2.5.

To meet these required standards and protect the public and the environment from dust emissions, surface filters are widely used in industrial gas cleaning for the separation of particles from dust-laden gas flows. They are commonly confectioned in the form of filter bags and installed in varying numbers in so-called baghouses. The filters generally operate with a high collection efficiency, since the dust-laden air passes through a large filter area where the separated dust forms a dust cake on the surface of the filter medium.

A sufficiently thick dust layer enables near-perfect particle separation and very low clean gas concentration, close to zero-emission. As the thickness of the dust cake increases, the pressure drop also rises. The cake is periodically removed from the surface of the filter bag to reduce the pressure drop and enable long-term economic operation. Regeneration occurs, e.g., via pulse-jet cleaning at fixed time intervals or at predetermined maximum differential pressure limits, commonly referred to as Δt[1)]-controlled and Δp-controlled modes of operation, respectively. The removal of the cake leads to a sharp increase in particle concentration in the clean gas immediately after regeneration, as particles may penetrate the filter medium for a short time. Upon the new formation of the cake, the particle concentration declines again.

1) List of symbols at the end of the paper.

[1]Camila R. de Lacerda, Prof. Dr. Mônica L. Aguiar
camilaraqueldelacerda@gmail.com
Federal University of São Carlos, Graduate Program of Chemical Engineering, Rodovia Washington Luís, s/n, 13565-905 São Carlos, SP, Brazil.

[2]Camila R. de Lacerda, Peter Bächler, Almuth D. Schwarz, Prof. Dr.-Ing. Achim Dittler
Karlsruhe Institute of Technology, Institute of Mechanical Process Engineering and Mechanics, Strasse Am Forum 8, 76131 Karlsruhe, Germany.

[3]Prof. Dr. Rafael Sartim
Global R&D Brazil, ArcelorMittal, Avenida Brigadeiro Eduardo Gomes, n° 526, Polo Industrial Tubarão, 29160-904 Serra, ES, Brazil.

[4]Prof. Dr. Rafael Sartim
Federal University of Espírito Santo, Department of Industrial Technology, Avenida Fernando Ferrari, 514, 29075-910 Goiabeiras, Vitória, ES, Brazil.

In addition to proper design and operation of the filter bag, sizing, installation, operating parameters, and maintenance, another important factor to consider when aiming to minimize emissions is the seam design of the filter bags. The filter medium itself is manufactured and sold by the meter. For the application in baghouses, confectioning of the filter medium is necessary so that filter elements, e.g., filter bags, can be installed in an efficient manner. Typical ways of confectioning are sewing, gluing or welding the filter material. Regarding sewn filter bags, the seam regions are potential leak points during the filtration process and can contribute to the overall dust emissions. The contribution of small leaks in surface filters to dust emissions has been studied in different ways, both for small coupons of the filter media in filter test rigs and for filter bags installed in pilot plant-scale baghouses, or in industrial plants.

Related to the evaluation of small coupons in filter test rigs, Bach et al. [7] investigated the behavior of different pinhole diameters ranging from 288 to 1041 μm in a filter coupon. The experiments and calculations showed that the larger the pinholes, the lower the collection efficiency of the filter sample. An increase in filter face velocity also led to a rise in collection efficiency of the filter medium with the pinhole, as a crater would form around the pinhole region, benefitting the inertial impaction mechanism of larger particles. With larger dust cake thickness, resistance to airflow and the velocity through the pinholes increase.

Mouret et al. [8] also evaluated the penetration of nanoparticles through filters perforated with defined pinholes. The results indicated that the smaller the particle diameter, the higher the penetration through the pinholes. This result was more pronounced for filters with high airflow resistance, as a larger fraction of the volume flow would pass through the pinhole instead of the fiber matrix. The authors developed a model to explain the experimental data, and the experiment was in good agreement with the model.

Mukhopadhyay and Mahawar [9] experimentally investigated the emission behavior of leaks over time with different hole diameters and the impact of the position of the hole, i.e., bottom and top of a vertical filter medium. The authors found results that an increase in the hole diameter from 1 to 2 mm, which corresponds to an enlargement of the leak surface area by a factor of four, causes the emission to increase by more than four times at both hole positions. However, when changing the hole diameter from 2 to 4 mm, an increment of the leak surface area by a factor of four was detected, and the emission increased by less than a factor of four in both positions. Li et al. [10] recently modeled and experimentally verified filtration in filter media with different leak ratios and pinhole diameters. The results demonstrated that leakage causes the collection efficiency to decrease.

Concerning investigations close to the industrial application, e.g., in pilot plant-scale baghouses, Mukhopadhyay and Choudhary [11] investigated the impact of the seamline spacing on emissions. The authors found that for a constant stitching technique and hole diameter, larger seamline spacings and larger medium overlapping areas lead to lower outlet emissions. Kurtz et al. [12] evaluated the contribution of small holes intentionally placed into filter bags, and the contribution of seams, on the particle emissions. The results showed that emissions were significantly increased even due to very small holes, and leaks from open seams accounted for 75 % of the filter medium emissions for free-flowing test dust.

Bächler et al. [13] investigated the particle emission contribution of individual filter bags by applying low-cost distributed sensors. The authors detected an increase in the total continuous emissions locally via the low-cost particulate matter sensor by replacing one out of nine sealed-seam filter bags with a filter bag made from a non-membrane filter medium with non-sealed seams. The filter bag with seamlines caused continuous particle emissions and concentration peaks with higher peak height after pulse-jet cleaning and could be spatially identified as an emission hotspot within the baghouse filter.

In a later investigation, Bächler et al. [14] examined the local particle emission through filter bags with three stitched seamlines and the corresponding particle emission evolution over multiple filtration cycles for different cleaning tank pressures, applying distributed low-cost particulate matter (PM) sensors. During the first stages of filter life, high continuous emissions could be detected for each installed filter element. After the initial cleaning cycles, the seams were presumably clogged and consequently, a reduction of the particulate emission level occurred. However, continuous emissions, indicating particle penetration through seams, still took place for individual filter bags, and they were more pronounced the higher the cleaning tank pressure. This behavior was associated with the removal of particles from the seam regions that were previously clogged, allowing the particles to penetrate the seam holes once again.

Regarding the investigation in industrial plants, Tomanovich and Knotts [15] visually detected dust bleeding through the seams of filter bags used in cement kiln baghouses. They attributed the leaks to cleaning pulses, the low quality of the sewing thread, and other stress that widened the holes and provided a preferential pathway for PM to pass through. The authors sealed the seams to achieve lower particle emission levels, and a visual inspection confirmed that, after over a year of operation, the seam tape was undamaged and that the compartment had stayed clean.

Different diameters of the needle used in sewing filter bags play an important role in the filtration performance. Depending on the needle size, small holes could potentially clog after sufficient operational time and no longer affect dust emissions, while larger holes could serve as a permanent bypass through the filter medium, similar to a pinhole, and cause continuous dust emissions. Since the systematic contribution of filter seams regarding particle emissions, especially the influence of the needle diameter, has not been reported in the literature, this work aims to investigate the seam influence on the filtration efficiency of the filter medium. Fractional separation efficiency and dust emissions during a filtration procedure (conditioning, aging, stabilization, and measurement phases) adapted from the Verein Deutscher Ingenieure (VDI) 3926 guideline [16] were analyzed in four different samples, one without seam and three samples with seam, sewn with different needle diameters (90, 100, and 130 μm).

2 Material and Methods

2.1 Filter Medium

The filter medium used in the experiments has a polyester base with a polytetrafluoroethylene (PTFE) membrane layer laminated onto its upstream side. The specifications of the filter medium without seam, provided by the manufacturer, are listed in Tab. 1. Since the goal of this investigation was to analyze the impact of the seam hole, a membrane filter medium serves as a solid reference due to the high separation efficiency and fast cake buildup. That way most particle emissions can be attributed to smaller membrane defects, respectively the seam holes of the filter medium.

Table 1. Specifications of the filter medium made from polyester with PTFE membrane, without seam.

Permeability at 200 Pa [L dm^{-2}min^{-1}]	Area weight [g m^{-2}]	Thickness [mm]
45	550	2

Four types of flat sheet circular coupons of this medium were used: one without seam and three samples each with a seam sewn with different needle diameters (90, 100, and 130 µm), as illustrated in Fig. 1. Filter coupons with seam were sewn once, without overlapping fabrics. Note that the seam holes do not correspond with the needle diameter. The seam has different characteristics compared to, e.g., a pinhole caused by flying sparks, where the fibers might melt and cause a continuous hole. For the seam, the fiber matrix adjacent to the seam hole is still intact and the seam hole is filled by sewing thread. This can serve as a base for bridging and clogging the defect.

In typical applications, with entire filter bags, the seam represents a smaller portion of the total filter area, when compared to a small circular sample, consequently leading to a different number of seam holes. According to Binnig et al. [17], the seam portion in a circular coupon corresponds to 14 % of the total filter area, while in an entire filter bag this value is only 3 %. Therefore, when transferring the results to an entire filter bag, there is a reduction in the difference between the media with and without a seam.

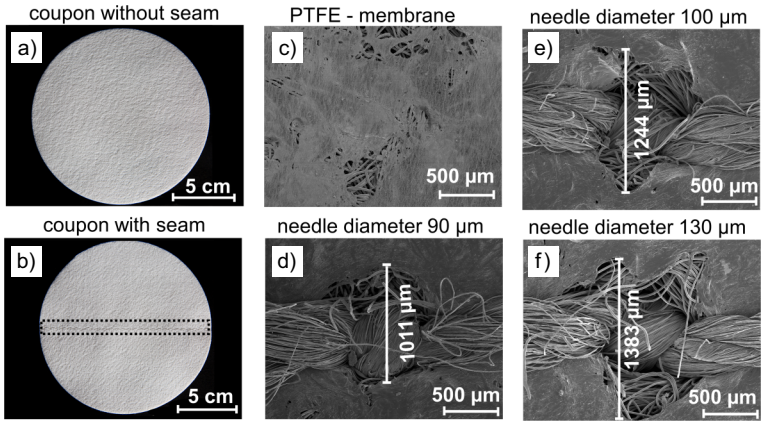

Figure 1. Full-scale photograph of the face side of the coupons without seam (a), with seam (b); SEM images of the PTFE membrane (c), and the seam holes associated with different needle diameters: 90 µm (d), 100 µm (e), 130 µm (f).

2.2 Experimental Procedure and Test Rigs

To investigate the fractional separation efficiency of the unloaded media samples, a commercially available MFP 3000 HF (Palas®), Fig. S1 (Supporting Information), with a U-SMPS (Palas®) to determine the particle size distributions and number concentrations was used. Detailed information about the procedure and this test rig can be found in the Supporting Information and in the work by Schwarz et al. [18]. To evaluate emission behavior during filtration and regeneration events over multiple cycles, a VDI 3926 test rig was employed, with an optical emission measurement consisting of a Promo® 2000 with a Welas® 2100 sensor from Palas®; see Fig. 2. More details about this optical device can be found in [19, 20].

2.2.1 VDI 3926 Test Rig

The operating parameters of the VDI 3926 test rig were maintained constant for all experiments: filter face velocity of 3.33 cm s^{-1}, raw gas concentration of 5 g m^{-3}, cleaning tank pressure of 5 bar, open valve for the pulse of 60 ms, and filter area of 176 cm^2 containing 28 exposed seam holes in the samples with seam.

A dust feeder disperses the test dust into a raw gas chamber, where an extinction measurement is installed as a monitor to ensure a constant concentration of the raw gas. The differential pressure between raw gas and clean gas side is monitored. When the predetermined maximum value of 1000 Pa is reached, a pressure pulse of 5 bar and 60 ms valve opening time is released to detach the dust cake.

The average mass concentration is only determined using the arithmetic mean of the real-time measurements gathered by the optical particle counter (Promo® 2000 with a Welas® 2100 sensor from Palas®). Typically, there is a good agreement regarding emission levels of gravimetrical and optical measurement; compare source Bächler et al. [21]. At the end of the clean gas duct is an isokinetic sampling probe for the Welas® 2100 sensor that allows real-time measurement of the mass concentrations and particle size of the penetrating aerosol every one second.

The applied filter test procedure consists of four subsequent stages, as displayed in Fig. 2. In the first stage, i.e., conditioning, the filter medium is subjected to 30 loading cycles with predetermined differential pressure for the pulse-jet cleaning. In the second stage, aging, the filter medium is subjected to 1000 cleaning pressure pulses at 30-s intervals each, thus causing frequent cake detachment, and enabling continuous emission through the filter medium, so that particles are deposited in the fiber

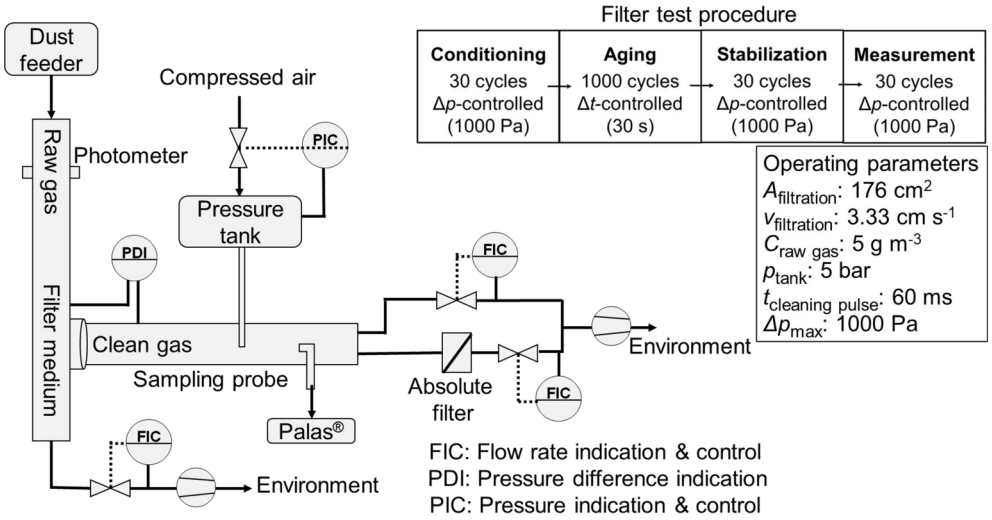

Figure 2. Flow diagram of the VDI 3926 test rig with the phases of the filter test procedure and operating parameters.

matrix. This effect called filter aging typically leads to an increase in residual differential pressure and better particle separation. The third stage, stabilization, is performed to stabilize the operating conditions, in which the filter medium is exposed to 30 loading cycles with predetermined differential pressure for the pulse-jet cleaning. In the last stage, measurement, the filter medium is again exposed to 30 filtration cycles with Δp-controlled operation to be able to compare the different media samples under equal conditions.

2.3 Test Aerosols

Two test dusts were used in the experiments. For an evaluation of the fractional separation efficiency under strict laboratory conditions, NaCl was employed since it can be easily dispersed with a narrow particle size distribution. Further information on the aerosol generation can be found in the Supporting Information.

For the investigation of filtration cycles, PURAL SB® was used since it is a nontoxic powder with good dispersive properties. It has a density of 2800 kg m^{-3}, a mass mean diameter of 45 µm, and a refractive index of 1.64 according to the manufacturer. The dust also contains particles in the submicron region and generally causes high particle emissions in filter tests due to its free-flowing, non-agglomerating behavior [22].

3 Results and Discussion

3.1 Fractional Separation Efficiency Evaluated in the MFP 3000 HF Test Rig

Fig. 3 shows the fractional separation efficiency of the four samples evaluated in the MFP 3000 HF test rig: one sample without seam and three samples sewn with different needle diameters (90, 100, and 130 µm).

The sample without seam exhibits separation efficiencies greater than 99 %, which is typical for membrane filter media.

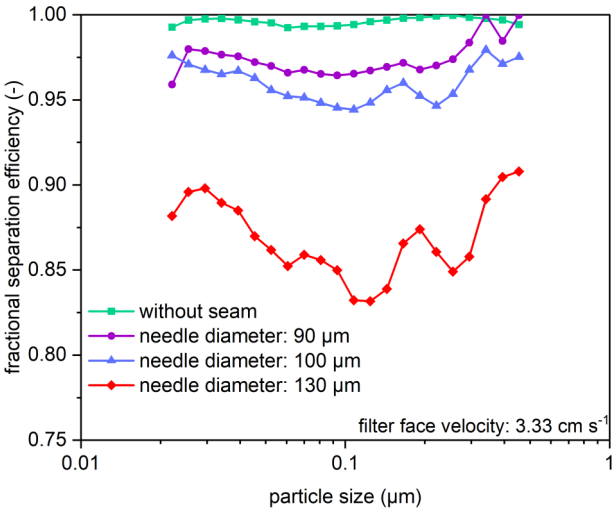

Figure 3. Fractional separation efficiency of the unloaded samples without seam and with seam (needle diameters of 90, 100, and 130 µm).

For the samples sewn, the larger the needle diameter, the larger the hole diameter, and the lower the fractional separation efficiency. These results are consistent with the works of Bach and Schmidt [7] and Mouret et al. [8], in which the authors evaluated different pinhole diameters in surface filters and found that bigger pinhole diameters lead to a marked reduction in filtration efficiency.

The holes in the samples with seam became preferential paths for the airflow and consequently, an increase in the interstitial velocity occurred. With rising velocity through the seam holes, the mechanism for collecting particles smaller than 0.1 µm by Brownian diffusion was impaired. However, for particles larger than 0.1 µm, the separation efficiency increased due to the larger role of inertial impaction, which was favored by the higher velocity through the holes and the higher inertia of the particles [7, 23, 24].

3.2 Influence of the Seams with Different Needle Diameters on the Filtration Cycle Progress and Differential Pressure in a VDI 3926 Test Rig

The conditioning is the first stage of the filter test procedure. The initial filtration cycles are unstable, where fluctuations of the residual pressure drop and cycle time may occur. Following the conditioning, aging, and stabilization, the measurement is the last stage of the procedure. At this stage, stable operating conditions are assured, and the comparison of the different filter media can be based on similar aging conditions for each sample.

Fig. 4a indicates the time it takes to complete 30 cycles. Fig. 4 b shows the initial pressure drop (Δp_0) of each sample, in the conditioning and the measurement stages. Both stages are a measure for filter aging. For a factory new filter medium, longer cycle times, respectively lower initial pressure drops, are expected.

Fig. 4a demonstrates that, in the conditioning stage, the total time required to complete 30 cycles is similar among all evaluated samples. The biggest difference is around 12 min between the sample without seam and the one with a needle diameter of 130 µm, approximately 24 s longer for each cycle. This is a small difference, considering that this stage is relatively unstable regarding the duration of the cycles. In the measurement stage, the time to complete 30 cycles is very similar among the three samples with seam. The sample without seam presented a much shorter time for the test procedure. This behavior of the sample without seam can be explained by the faster increase of pressure drop, since the sample collects more dust, as was shown by the evaluation of the fractional separation efficiency in Fig. 3. In the samples with seam, in addition to the flow through the membrane layer and the fiber matrix, there are seam holes, which make the filter medium more permeable and favor direct penetration of the particulate material. This impacts filter loading, causing the filter medium to load slower and thus take longer to reach the maximum pressure of cleaning and completion of the filtration cycle.

Fig. 4b validates the observations for the time to complete 30 cycles. The filter medium without seam shows a higher pressure drop in both stages of conditioning and measurement compared to the samples with a seam. The differences between the samples with seam amount to single-digit Pascal and are negligible.

These results demonstrate that the presence of a seam slightly influences the filtration progress, which can be shown by both, the time required to complete the filtration cycles and the residual pressure drop of the filter media. When comparing the results between the samples with seam, it can be noted that the needle diameter does not have a great influence on the operating performance, respectively differential pressure, of the filter.

3.3 Emissions During Conditioning, Aging, Stabilization, and Measurement Stages

Figs. 5a–d illustrate the optically determined total particle number concentration over time for each of the four samples types (without seam, with needle diameters of 90, 100, and 130 µm), during the conditioning (Δp-controlled), aging (Δt-controlled), stabilization (Δp-controlled), and measurement (Δp-controlled) stages, respectively. For the aging stage (Fig. 5b), the scale is different for each sample to enable visualization of the 1-min averaged values.

Analyzing Fig. 5a, i.e, conditioning stage, the sample without seam has near-zero emission level and low concentration peaks after pulse-jet cleaning, even in the first minutes, demonstrating the high separation efficiency of the membrane filter medium. The average number concentration for the 30 cycles was approximately 7.13 # cm^{-3}. The higher values of the concentration peaks during the first 100 min occur because the pores and small defects of the filter medium are not yet clogged. After the initial 200 min of the experiment, barely any dust emission can be detected. The sewn samples with needle diameters of 90, 100, and 130 µm indicate initial particle penetration (shown by light grey rectangles in the graphs). The sample without seam did not have this initial peak demonstrating the high separation efficiency of the mostly intact membrane layer.

The samples with seam holes also show higher concentration peaks after the cleaning pulses over the whole experimental period. The average number concentrations for 30 cycles were 14.74, 124.83, and 107.33 # cm^{-3} for the samples sewn with needle diameters of 90, 100, and 130 µm, respectively. In this conditioning phase, one would expect the height of the concentration peaks to decrease over several cycles due to the pores and seam holes being clogged by particulate matter, but the sewn

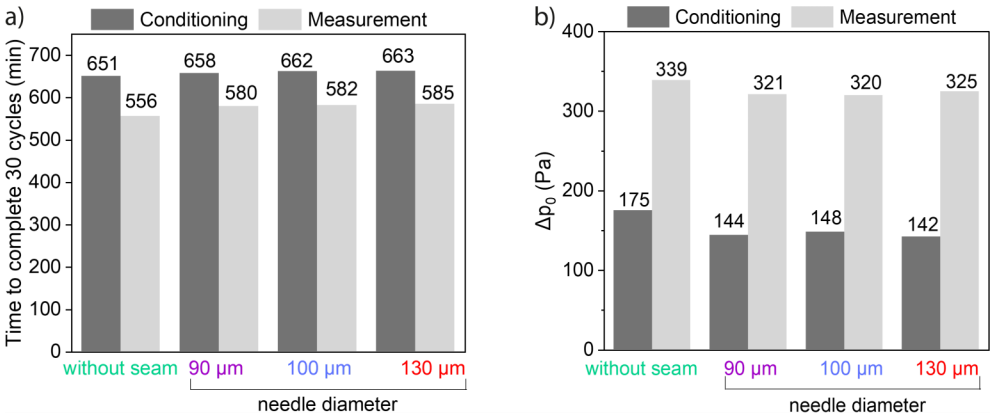

Figure 4. Time to complete 30 cycles (a) and initial pressure drop (Δp_0) (b) at 3.33 cm s^{-1} filter face velocity, for each sample, in the conditioning and measurement stages.

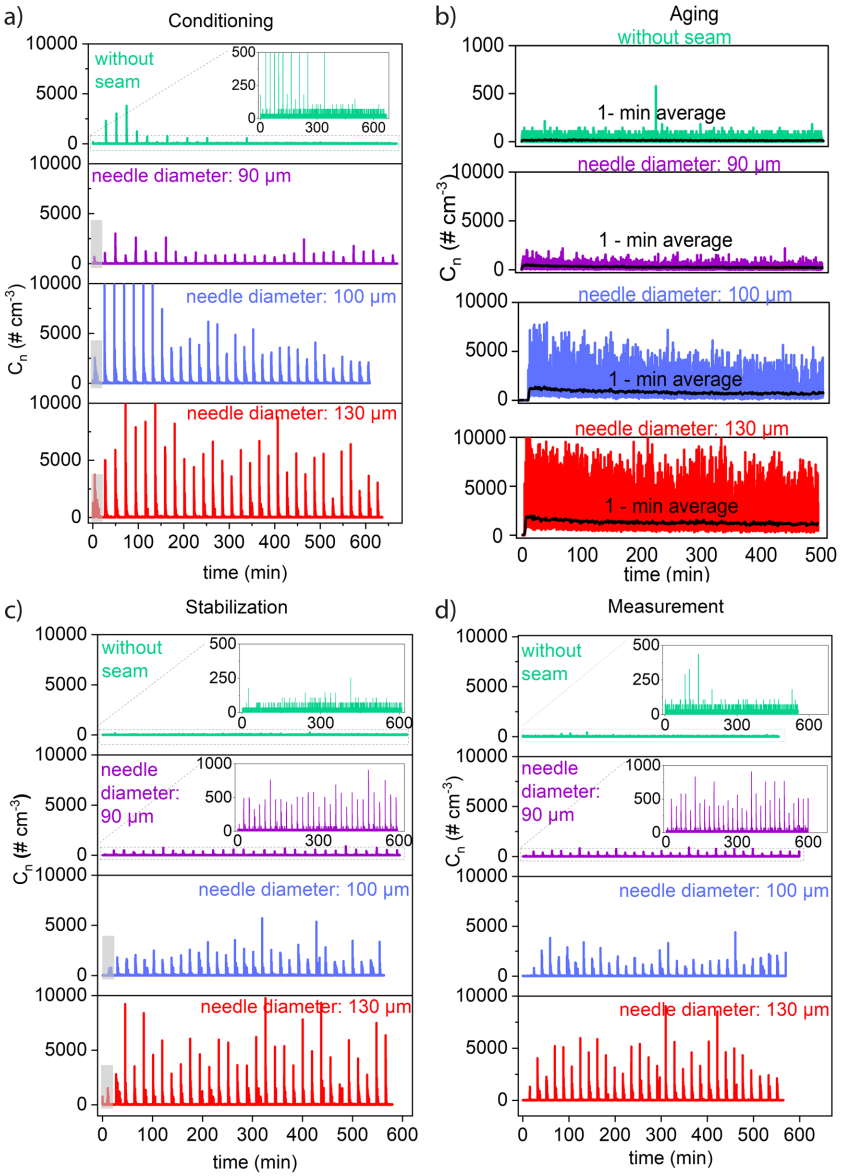

Figure 5. Particle number concentration over time for the samples without seam (green) and with needle diameters of 90 µm (purple), 100 µm (blue), and 130 µm (red), during conditioning (a), aging (b), stabilization (c), and measurement (d) stages. For the aging stage (b), the 1-min averaged values are also shown. The light grey rectangles represent the peaks before the first cleaning pulse.

samples show scattering in peak height. This can be explained mainly by the unstable conditions during the initial cycles. Note that the sample with a needle diameter of 100 µm might have the highest average emission concentration due to the large peak concentrations in the first 100 min, but after 200 min of the experiment, the peak height is lower compared to the sample with 130 µm needle diameter.

Fig. 5b shows the aging stage of each sample. The aim of this stage is to generate comparable conditions, which are closer to those that filters endure during industrial application after a longer period of operation. During the aging stage, there is no complete dust cake formation since the cycles are short. Consequently, constant emissions of particulate matter are detected on the clean gas side due to the continuous penetration of particles. In this stage, despite the high emissions, there is also the aggregation of particulate matter inside the filter medium. The deposited particles enhance the collection efficiency of the filters, lowering the emission concentration, as can be seen by the decreasing behavior of the 1-min average curve (black). The average number concentrations during the 1000 cycles of 30 s each were 12.74, 292.90, 795.79, and 1306.43 # cm^{-3} for the samples without seam, with needle diameters of 90, 100, and 130 µm, respectively, showing that larger needle diameters lead to higher emission levels and that the seam holes have a strong influence on the emissions.

In Fig. 5c, stabilization stage, the sample without seam shows very low emissions, mostly below 100 # cm^{-3} during all cycles. Concentration peaks after pulse-jet cleaning cannot be distinguished from this "baseline" emission level, as can be observed in the detailed view. Note that the overall number concentration detected by the Palas® reference is calculated from singular counting events. A concentration of 33 # cm^{-3} corresponds to a single particle count (100 # cm^{-3} ≈ 3 counts). The detected counts during this period can be allocated to the lower size fractions of the optical particle counter (below 300 nm), where the accuracy of the device drops [14]. Thus, the continuous emission detected for the sample without seam and during the conditioning phase with an established dust cake, (Fig. 5a, green), corresponds to almost perfect particle separation over the whole experiment. The emissions from the samples with seam are lower compared to the conditioning phase (Fig. 5a), due to the aging step.

The transient emissions after the cleaning pulses are still fluctuating in peak height mainly for the samples with a needle diameter of 100 and 130 µm, where some peaks of the final cycles were higher than the initial ones. In addition, it is noted that for samples with needle diameters of 100 and 130 µm there still occurs a particle emission peak due to initial penetration at the beginning of the cycle, depicted by the light grey rectangles, before the first cleaning pulse. This shows that at this stage the holes of the seam were still open and prone to direct penetration after aging. During the pulse they expanded, leading to higher (higher peak emission) and wider (emission detected over a longer period) peaks. The average number concentrations for 30 cycles were 4.33, 9.36, 60.74, and 105.65 # cm^{-3} for the samples without seam, with needle diameters of 90, 100, and 130 µm, respectively.

Fig. 5d, measurement stage, the last stage of the procedure, no major changes are observed for samples without seam and with needle diameter of 90 µm, when compared to the stabilization stage (Fig. 5c). Nevertheless, the samples with needle diameters of 100 and 130 µm continue to present a decline in particle emissions, mainly regarding the concentration peaks. The average number concentrations for 30 cycles were 5.43, 10.30, 55.15, and 85.91 # cm^{-3} for the samples without seam and with needle diameters of 90, 100, and 130 µm, respectively. After the four stages of the procedure, i.e., conditioning, aging, stabilization, and measurement, the emissions of the samples with larger needle diameters of 100 and 130 µm still have a major impact on the seam regarding the dust emissions. The samples without seam and with a needle diameter of 90 µm show similar values to those of the stabilization phase, demonstrating that these samples reached an average emissions stability, i.e., clogging of the seams and asymptotic behavior of the particle emission.

3.4 Particle Size Distribution in the Clean Gas During Conditioning and Measurement Stages

Fig. 6 illustrates the particle size distribution on the clean gas side for each sample evaluated, without seam and with seam (with needle diameters of 90, 100, and 130 µm) in the first and last stages of the filtration procedure, conditioning (Fig. 6a) and measurement (Fig. 6b), respectively. Evaluating the particle size distribution in these two stages, the mainly submicron emissions change over the duration of the procedure for the different needle diameters. The clean gas concentrations are higher for the samples with bigger seam holes in both stages. In comparison with the sample without seam, not only does the direct penetration mechanism through the pores of the filter medium occur, but also the bypass through the holes of the seam takes place. For larger seam holes there is less inertial impaction, and thus coarser spectra of the particles can penetrate to the clean gas side. These results agree with the results found by Bach and Schmidt [7] when analyzing pinholes with defined diameters.

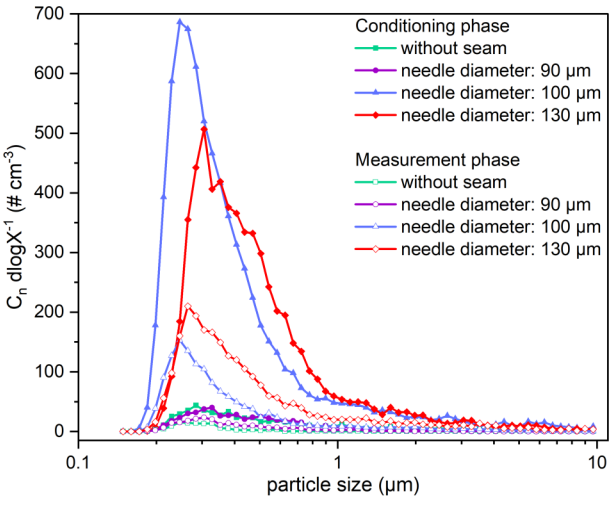

Figure 6. Size distribution of PURAL SB® emission measured via Palas® system in the clean gas side during the first 90 min of the conditioning (a) and the measurement (b) stages.

When evaluating different pinholes sizes, the authors found that larger pinholes lead to coarser spectra. The samples without seam and with seam with a needle diameter of 90 µm show a very similar size distribution in both phases. In the sample with a needle diameter of 90 µm, the interstitial velocity increases considerably in the holes of the seam and favors the inertial impact collection mechanism, which makes the collection of particles in this size range more efficient. The reason for the higher concentration level of the 100-µm sample compared to the 130-µm sample during conditioning corresponds to the initially higher emission peaks detected during this phase (compare Fig. 5a).

3.5 Development of Average Mass Concentration over the Filter Test Procedure

The average mass concentrations for each stage of the filter test procedure are presented for each sample in Fig. 7, where the different emission levels of the four filter samples can be clearly distinguished. The average mass concentrations of the samples with seam are higher for larger needle diameters in all stages of the filter test procedure.

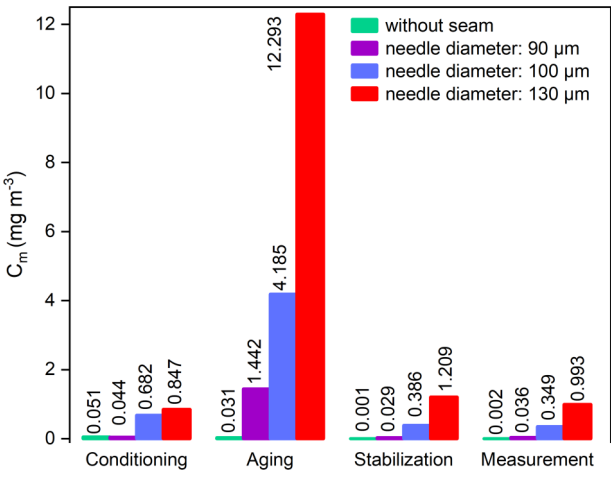

Figure 7. Average mass concentration during the conditioning, aging, stabilization, and measurement stages for each sample evaluated.

The sample without seam presents a reduction in the average mass concentration because the pores and smaller defects of the membrane layer of the filter medium are clogged over the procedure and the larger particles are no longer able to penetrate the filter medium. In samples with seam holes, besides the direct penetration mechanism through the filter medium, there occurs also penetration through the seam holes. The sample with a needle diameter of 130 µm even presented an increase in the average mass concentration from the conditioning stage to the measurement stage, showing that this sample still faces a

strong influence of the seam regarding the emissions, which means that the whole filtration procedure including the four stages was not enough to seal the seam holes permanently or even improve particle separation.

Further information depicting the pressure buildup and outlet mass concentration, for the samples without seam and with needle diameter of 130 µm, can be found in the Supporting Information.

4 Conclusion

The contribution to particle emissions through filter seams with different needle diameters (90, 100, and 130 µm) and one filter without seam (membrane filter medium) was investigated in terms of fractional separation efficiency and during a filtration procedure from the VDI 3926 guideline (conditioning, aging, stabilization, and measurement). Regarding the fractional separation efficiency, the results indicated that bigger needle diameters lead to lower fractional separation efficiencies, and the sample without seam presented the highest efficiency (near-perfect separation).

The comparison of the four samples with respect to the conditioning and the measurement phases showed that the evaluated needle diameters had a negligible influence on the time required to complete the filtration cycles and the differential pressure; however, there was a slight influence between the sample without seam and the others with seam holes. When analyzing the four samples with respect to emissions (number concentration over time during the four phases of the filtration procedure), it was observed that the samples without seam and with needle diameter of 90 µm reached an average emission stability (lower fluctuation in peak height) throughout the procedure. The samples with needle diameters of 100 and 130 µm continued to show a higher influence of the seam on the emissions.

Concerning the particle size distribution on the clean gas side during the first and the last stages, conditioning and measurement, respectively, it was noted that the clean gas number concentration was higher for the two samples with bigger needle diameters (100 and 130 µm), while the particle number concentrations of the samples without seam and with needle diameter of 90 µm were pretty similar due to the favored inertial impaction collection mechanism in the sample with a needle diameter of 90 µm. The last comparison was related to the development of the mass concentration over the filtration procedure, where the emission levels of each filter medium were clearly distinguished due to the different behaviors of penetration through the pores and the seam holes.

The results indicate a strong influence of the needle diameter in filter bag design. Sealed or taped seams can improve the separation efficiency of the filter element. While there might be a significant loss of filter area in the case of larger amounts of filter bags, the potential benefits for the dust emissions probably outweigh additional investment costs when considering environmental aspects.

Supporting Information

Supporting Information for this article can be found under DOI: https://doi.org/10.1002/ceat.202200132.

Acknowledgment

This work was financed by Coordenação de Aperfeiçoamento de Pessoal de Nível Superior – Brasil (CAPES), Finance Code 001, grant no 88887.486170/2020–00; ArcelorMittal, grant no. 44/2015; Conselho Nacional de Desenvolvimento Científico e Tecnológico (CNPq), grant no. 142086/2019–3; and Fundação de Amparo à Pesquisa do Estado de São Paulo (FAPESP), grant no. 97/04024–7. We acknowledge the cooperation of Junker Filter GmbH for providing the filter samples. Open access funding enabled and organized by Projekt DEAL. [Correction added on October 04, 2022, after first online publication: Projekt Deal funding statement has been added.]

The authors have declared no conflict of interest.

Symbols used

A	[m^2]	area
C_m	[$g\ m^{-3}$]	mass concentration
C_n	[$\#\ cm^{-3}$]	number concentration
p	[Pa]	pressure
Δp_0	[Pa]	initial differential pressure
Δp_{max}	[Pa]	maximum differential pressure
Q	[$L\ min^{-1}$]	volumetric flow
RH	[%]	relative humidity
T	[°C]	temperature
t	[s]	time
v	[$m\ s^{-1}$]	velocity

Abbreviations

CONAMA	Conselho Nacional de Meio Ambiente
FIC	flow rate indication and control
MC	moisture control
MFP	modular filter test system
MPPS	most penetrating particle size
PDI	pressure difference indication
PDR	differential pressure regulation
PIC	pressure indication and control
PM	particulate matter
PTFE	polytetrafluoroethylene
SEM	scanning electron microscopy
TA	technische Anleitung
TC	temperature control
U-SMPS	universal scanning mobility particle sizer
VDI	Verein Deutscher Ingenieure

References

[1] https://www.euro.who.int/_data/assets/pdf_file/0004/193108/REVIHAAP-Final-technical-report-final-version.pdf (Accessed on February 27, 2022)

[2] D. M. Teleanu, C. Chircov, A. M. Grumezescu, A. Volceanov, R. I. Teleanu, *J. Clin. Med.* **2018**, *7*, 490. DOI: https://doi.org/10.3390/jcm7120490

[3] L. C. Garcidueñas, A. G. Maciel, P. S. Mukherjee, R. R. Robles, B. P. Guillé, C. G. Chávez, R. T. Jardón, J. V. Cross, I. A. M. Ahmed, V. V. Karloukovski, B. A. Maher, *Environ. Res.* **2019**, *176*, 108567. DOI: https://doi.org/10.1016/j.envres.2019.108567

[4] http://www.verwaltungsvorschriften-im internet.de/bsvwvbund_18082021_IGI25025005.htm (Accessed on February 27, 2022)

[5] http://www.dca.iag.usp.br/material/fornaro/ACA410/Resolucao_CONAMA_491_2018.pdf (Accessed on February 27, 2022)

[6] https://www.euro.who.int/_data/assets/pdf_file/0005/78638/E90038.pdf (Accessed on February 27, 2022)

[7] B. Bach, E. Schmidt, *J. Hazard. Mater.* **2007**, *7*, 235–239. DOI: https://doi.org/10.1016/j.jhazmat.2007.01.093

[8] G. Mouret, D. Thomas, S. Chazelet, J. C. A. Collin, D. Bemer, *Aerosol Sci.* **2009**, *40*, 762–775. DOI: https://doi.org/10.1016/j.jaerosci.2009.04.010

[9] A. Mukhopadhyay, G. Mahawar, *Indian J. Fibre Text. Res.* **2020**, *45*, 326–331.

[10] J. Li, Q. Wu, Y. Huang, Z. Sun, J. Li, D. Wu, *Process Saf. Environ. Prot.* **2022**, *158*, 282–290. DOI: https://doi.org/10.1016/j.psep.2021.12.012

[11] A. Mukhopadhyay, A. K. Choudhary, *Part. Sci. Technol.* **2013**, *31*, 632–642. DOI: https://doi.org/10.1080/02726351.2013.831152

[12] O. Kurtz, J. Meyer, G. Kasper, *Particuology* **2017**, *30*, 40–52. DOI: https://doi.org/10.1016/j.partic.2016.08.001

[13] P. Bächler, J. Szabadi, J. Meyer, A. Dittler, *J. Aerosol Sci.* **2020**, *150*, 105644. DOI: https://doi.org/10.1016/j.jaerosci.2020.105644

[14] P. Bächler, V. Löschner, J. Meyer, A. Dittler, *Proc. Saf. Environ. Technol.* **2022**, *160*, 411–423. DOI: https://doi.org/10.1016/j.psep.2022.02.005

[15] J. Tomanovich, J. Knotts, in *Proc. of the Cement Industry Technical Conf.*, Institute of Electrical and Electronics Engineers (IEEE), Orlando, FL **2013**, 1–21.

[16] VDI 3926 Part 1, *Testing of cleanable filter media*, Düsseldorf **2004**.

[17] J. Binnig, J. Meyer, G. Kasper, *Powder Technol.* **2009**, *189*, 108–114. DOI: https://doi.org/10.1016/j.powtec.2008.06.012

[18] A. D. Schwarz, J. Dutzi, P. Weber, C. Sattler, K. Schulz, T. Caesar, J. Meyer, A. Dittler, *Chem. Eng. Technol.* **2022**, *45*, 43–50. DOI: https://doi.org/10.1002/ceat.202100344

[19] https://www.palas.de/product/promo2000 (Accessed on February 21, 2022).

[20] https://www.palas.de/en/product/aerosolsensorwelas2100 (Accessed on February 21, 2022)

[21] P. Bächler, J. Meyer, A. Dittler, *Gefahrstoffe - Reinhalt. Luft.* **2019**, *79*, 443–450. DOI: https://doi.org/10.37544/0949-8036-2019-11-12-49

[22] P. Bächler, J. Meyer, A. Dittler, *Aerosol Sci. Technol.* **2022**, *56 (4)*, 394–402. DOI: https://doi.org/10.1080/02786826.2022.2027335

[23] W. C. Hinds, *Aerosol Technology: Properties, Behavior, and Measurement of Airborne Particles*, John Wiley & Sons, New York **1999**.

[24] R. Boudhan, A. Joubert, K. Gueraoui, S. Durécu, D. Venditti, D. T. Tran, L. Le Coq, *Waste Biomass Valor.* **2018**, *9*, 731–737. DOI: https://doi.org/10.1007/s12649-017-9858-4

